Engineering Notes

Optimal Combination of Magnetic Attitude Control with Impulsive Thrusting

Behrad Vatankhahghadim[*] and Christopher J. Damaren[†]
University of Toronto, Toronto, Ontario M3H 5T6, Canada

A	=	cross-sectional area of magnetic torquers, m^2
a	=	semimajor axis, m
$\boldsymbol{b}$	=	magnetic field vector, T
C	=	rotation matrix between two frames
d	=	coil diameter of magnetic torquers, m
E	=	energy consumption of magnetic torquers, MJ
e	=	eccentricity
$\boldsymbol{I}$	=	moment of inertia matrix, $kg \cdot m^2$
$\boldsymbol{i}$	=	coil current in magnetic torquers, A
i	=	inclination, rad
k	=	control gain used for reference proportional-derivative controller
$\boldsymbol{m}$	=	magnetic dipole moment vector, $A \cdot m^2$
N	=	total number of impulses
$\hat{N}$	=	number of impulses per orbit
$\boldsymbol{n}$	=	gain of impulsive thrust vector, $N \cdot m$
n	=	number of turns per coil in magnetic torquers
$\boldsymbol{r}$	=	position vector, m
T	=	orbital period, s
t_0	=	time of perigee passage, s
W	=	controllability Gramian matrix
γ	=	scaling factor for reference proportional-derivative controller
$\delta(t)$	=	Dirac delta function
$\boldsymbol{\epsilon}$	=	vector part of quaternions
η	=	scalar part of quaternions
$\boldsymbol{\theta}$	=	attitude Euler angle vector, rad
μ	=	standard gravitational parameter, m^3/s^2
Ξ	=	hybrid state transition matrix
$\boldsymbol{\tau}$	=	torque vector, $N \cdot m$
Φ	=	continuous-time state transition matrix
ϕ	=	angle from Euler axis-angle parameters, rad
Ψ	=	discrete-time state transition matrix
Ω	=	right ascension of ascending node, rad
$\boldsymbol{\omega}$	=	angular velocity vector, rad/s
ω	=	argument of periapsis, rad
$\mathbf{1}_{n \times n}$	=	$n \times n$ identity matrix
$\mathbf{0}_{m \times n}$	=	$m \times n$ zero matrix

$(\dot{\cdot})$	=	differentiation with respect to time
$|\cdot|$	=	Euclidean norm of a vector
$\|\cdot\|$	=	root-mean-square norm of a quantity
$(\cdot)^\times$	=	skew-symmetric matrix operator

Subscripts

B	=	in body-fixed reference frame
c	=	continuous time
d	=	discrete time
dist	=	disturbance
e	=	equilibrium value
f	=	final value
G	=	in Earth-centered inertial reference frame
imp	=	impulsive
mag	=	magnetic
max	=	maximum among a set
nT	=	computed over n orbital periods
p	=	proportional gain
v	=	derivative gain
0	=	initial value

Superscripts

$(\cdot)^*$	=	optimal quantity
$(\cdot)^+$	=	postimpulse quantity
$(\cdot)^-$	=	preimpulse quantity

I. Introduction

THE interaction between Earth's magnetic field and the electromagnetic dipole moments resulting from electrical current flowing through the coils of a spacecraft's magnetic torquers can be used as a means to generate torques for attitude control purposes [1]. Although this mechanism has been under extensive study (a survey of which is provided in [2]) as an efficient approach for performing attitude control on near-Earth spacecraft, magnetic actuation alone results in instantaneous underactuation because the resultant torque is always perpendicular to the magnetic field vector due to the cross product from which it is obtained.

In the case of the attitude control problem, the pointwise un-controllability issue can be resolved by averaging over a period of time, owing to the time-varying nature of the magnetic field [2–4]; however, magnetic control suffers from a fundamental gain limitation, as demonstrated in [4], in which stability was proven to be guaranteed only if the feedback gains were within a certain bound. The need to alleviate this limitation, as well as a desire to allow for optimizations resulting in power savings and improved control performance, motivate the augmentation of magnetic control with an auxiliary impulsive thrust mechanism, hence yielding a continuous/impulsive control scheme that will be called a "hybrid" controller hereafter.

As an extension of earlier linear approaches for designing magnetic attitude controllers, various time-varying controllers were developed in [3], including some that relied on the solution of the periodic Riccati equation. Exploiting the quasi-periodic nature of the problem, [5] also proposed state-feedback control using an asymptotic linear quadratic regulator (LQR). Purely magnetic actuation's global stabilization based on the application of averaging theory to the time-varying system under consideration was studied in [6].

This Note aims to develop and study the stability of an optimal hybrid control scheme in which magnetic torquers and impulsive thrusters work in tandem and in an optimal manner, as they are

designed using the so-called hybrid LQR approach described in [7]. Simultaneous use of magnetic control and three-axis actuation (such as that provided by reaction wheels) as a hybrid mechanism, as well as the associated stability issues, were previously investigated in [8]. This was followed by a geometric technique for control vector decomposition presented in [9] that further built upon the idea of hybrid control but focused on the use of reaction wheels, which also provided continuous torques. In contrast, the design approach presented here uses impulsive thrusting to complement the magnetic controller in order to overcome the aforementioned gain limitation issues associated with a continuous feedback controller. The problem considered in this document is also fundamentally different from that in [9], as the latter attempts to judiciously decompose a given control signal into magnetic and three-axis portions, whereas the aim of this Note is to optimize the two actuation control inputs to be used together.

A hybrid continuous/impulsive attitude control problem similar to this project's was considered in [10], but one of their approaches used a linear time-invariant design technique with control allocation. Their other approach was based on an averaging assumption for a linear time-periodic approximation of the system and involved addition of impulsive actuators after a simple stabilizing magnetic feedback was designed. This was as opposed to designing the two portions of a time-varying controller simultaneously, as is accomplished in this work.

The concept of optimal continuous/impulsive control was recently applied in the context of spacecraft formation flight in [7], in which an optimal combined use of impulsive thrusting and Lorentz force actuation based on a continuous/discrete LQR was proposed. Although the dynamics of attitude control are different from those of formation flight, the controller design approach suggested in [7] is still applicable to and used in this work. That approach has also been further improved here by suggesting a more justifiable means of selecting the impulse application times based on a study of the system's pointwise controllability over small sliding time windows: using this approach, the thrusters will only be activated when the magnetic controller is least effective, hence resulting in potentially better control performance. Optimizing the cost function with respect to impulse times is not within the scope of this Note. Moreover, another contribution of this Note is an extension of the Floquet analysis (the classical version of which was used in [3,5,11] to check the closed-loop stability of LQR controllers for time-periodic models) to hybrid systems that also incorporate jump dynamics by using the novel concept of a hybrid state transition matrix.

This Note is organized as follows: First, the mathematical model used to describe the kinematics and dynamics of a spacecraft subject to magnetic and impulsive control torques and major disturbance torques is described in Sec. II. Then, the methodology used to design an optimal hybrid controller is summarized in Sec. III after a brief description on the model's linearization, and a controllability-based technique for selecting the impulse application times is presented. The concept of hybrid linear stability analysis is then explained, and a modified version of the Floquet theorem that suits the hybrid system of interest is proven in Sec. IV. Lastly, some numerical examples are considered in Sec. V, where the performance and stability of the proposed controller are studied, followed by some concluding remarks in Sec. VI.

II. Spacecraft Kinematics and Dynamics

The rotational dynamics are modeled using Euler's rigid-body equation [12]:

$$I\dot{\boldsymbol{\omega}} + \boldsymbol{\omega}^\times I\boldsymbol{\omega} = \boldsymbol{\tau}_{\mathrm{mag}} + \boldsymbol{\tau}_{\mathrm{imp}} + \boldsymbol{\tau}_{\mathrm{dist}} \tag{1}$$

where the applied torque on the right-hand side consists of $\boldsymbol{\tau}_{\mathrm{mag}}$ produced by magnetic torquers, $\boldsymbol{\tau}_{\mathrm{imp}}$ produced by impulsive thrusters, and $\boldsymbol{\tau}_{\mathrm{dist}}$ produced by external disturbance sources. The skew-symmetric operator $(\cdot)^\times$ acts on $\boldsymbol{\omega}$ as follows:

$$\boldsymbol{\omega}^\times = \begin{bmatrix} 0 & -\omega_3 & \omega_2 \\ \omega_3 & 0 & -\omega_1 \\ -\omega_2 & \omega_1 & 0 \end{bmatrix} \tag{2}$$

Assuming the impulses are applied at times t_k, $k \in \{1, 2, \cdots, N\}$, and taking into account only the gravity-gradient disturbances and residual magnetic dipoles resulting from onboard electronics (as these two are expected to be the most dominant sources of disturbance for near-Earth small spacecraft), these torque contributions can be represented as follows ([12] chapter 9):

$$\boldsymbol{\tau}_{\mathrm{mag}} = \boldsymbol{m}^\times \boldsymbol{b}_B \tag{3a}$$

$$\boldsymbol{\tau}_{\mathrm{imp}} = \sum_{k=1}^{N} \boldsymbol{n}_k \delta(t - t_k) \tag{3b}$$

$$\boldsymbol{\tau}_{\mathrm{dist}} = \frac{3\mu}{|\boldsymbol{r}_B|^5} \boldsymbol{r}_B^\times I \boldsymbol{r}_B + \boldsymbol{m}_{\mathrm{dist}}^\times \boldsymbol{b}_B \tag{3c}$$

where $\mu = 3.9859 \times 10^{14}$ m³/s² for Earth. The vectors expressed in the body-fixed frame can also be rewritten in terms of their inertial frame representations as $\boldsymbol{b}_B = \boldsymbol{C}_{BG} \boldsymbol{b}_G$ and $\boldsymbol{r}_B = \boldsymbol{C}_{BG} \boldsymbol{r}_G$, where $\boldsymbol{C}_{BG}$ denotes the rotation matrix from the inertial frame to the body-fixed frame. The magnetic field vector $\boldsymbol{b}_G$ can be estimated using a tilted dipole model of Earth's magnetic field, described in appendix H of [1] (a concise presentation of which can be found in [8]). To determine the position vector $\boldsymbol{r}_G$, a Keplerian orbit is assumed, and based on the well-known relationships that describe such orbits, the radial distance is determined as a function of true anomaly. The attitude of the spacecraft is represented using the singularity-free four-parameter set of quaternions, $\boldsymbol{\epsilon} = [\epsilon_1 \ \ \epsilon_2 \ \ \epsilon_3]^T$ and η, subject to the orthogonality constraint $\boldsymbol{\epsilon}^T \boldsymbol{\epsilon} + \eta^2 = 1$. Using the quaternions, the rotation matrix $\boldsymbol{C}_{BG}$ can be computed at all times ([12] chapter 2):

$$\boldsymbol{C}_{BG} = (\eta^2 - \boldsymbol{\epsilon}^T \boldsymbol{\epsilon}) \mathbf{1}_{3\times3} + 2\boldsymbol{\epsilon}\boldsymbol{\epsilon}^T - 2\eta\boldsymbol{\epsilon}^\times \tag{4}$$

The rotational kinematics are based on the well-known relationships between angular velocity and the quaternions' rates of change, which are in turn derived from the definition of angular velocity in terms of transformation matrices ([12] chapter 2):

$$\begin{bmatrix} \dot{\boldsymbol{\epsilon}} \\ \dot{\eta} \end{bmatrix} = \frac{1}{2} \begin{bmatrix} \eta \mathbf{1}_{3\times3} + \boldsymbol{\epsilon}^\times \\ -\boldsymbol{\epsilon}^T \end{bmatrix} \boldsymbol{\omega} \tag{5}$$

The nonlinear differential equations in Eqs. (1) and (5) fully describe the attitude motion of the spacecraft, and they must be simultaneously integrated over time to simulate the changes in attitude.

III. Optimal Hybrid Magnetic Control

To mitigate the pointwise uncontrollability issue associated with a solely magnetic controller, and in an attempt to overcome its fundamental gain limitation caused by the time-varying nature of the magnetic field (as demonstrated in [4]), the magnetic actuators are augmented with impulsive thrusters to form a hybrid (continuous/impulsive) control scheme. For a reasonable selection of the fixed impulse application times, pointwise controllability of the system can be assessed and used to determine the times at which the least control authority is provided by the magnetic actuators. This approach for selecting the impulse times does not aim to address controllability issues similar to those in [7] because, despite instantaneous underactuation, the system in this Note is, on average, controllable (as mentioned in Sec. I); instead, the motivation behind this approach is to employ the thrusters only at the time instances at which the magnetic controller is least effective.

To combine magnetic actuation and impulsive thrusting in an optimal manner, the continuous/impulsive linear quadratic regulator formulation developed for formation flight, described in [7], is applied to the attitude control problem at hand. This approach

involves defining a hybrid performance index that accounts for both continuous- and discrete-time control and state penalties, as well as determining the optimal control laws by solving the continuous- and discrete-time Riccati equations in tandem.

A. Linearization of the Model

Before proceeding with the hybrid LQR approach, the model (described by the dynamics presented in Sec. II) is first linearized ([12] chapter 4):

$$
\underbrace{\begin{bmatrix} \dot{\boldsymbol{\theta}}(t) \\ \ddot{\boldsymbol{\theta}}(t) \end{bmatrix}}_{\dot{\boldsymbol{x}}(t)} \simeq \underbrace{\begin{bmatrix} \boldsymbol{0}_{3\times3} & \boldsymbol{1}_{3\times3} \\ \boldsymbol{0}_{3\times3} & \boldsymbol{0}_{3\times3} \end{bmatrix}}_{\boldsymbol{A}_c} \underbrace{\begin{bmatrix} \boldsymbol{\theta}(t) \\ \dot{\boldsymbol{\theta}}(t) \end{bmatrix}}_{\boldsymbol{x}(t)} + \underbrace{\begin{bmatrix} \boldsymbol{0}_{3\times3} \\ -\boldsymbol{I}^{-1}\boldsymbol{b}_G^{\times}(t) \end{bmatrix}}_{\boldsymbol{B}_c(t)} \underbrace{[\boldsymbol{m}(t)]}_{\boldsymbol{u}(t)}, \quad t \neq t_k
$$

(6a)

$$
\underbrace{\begin{bmatrix} \dot{\boldsymbol{\theta}}(t_k^+) \\ \ddot{\boldsymbol{\theta}}(t_k^+) \end{bmatrix}}_{\boldsymbol{x}(t_k^+)} \approx \underbrace{\begin{bmatrix} \boldsymbol{1}_{3\times3} & \boldsymbol{0}_{3\times3} \\ \boldsymbol{0}_{3\times3} & \boldsymbol{1}_{3\times3} \end{bmatrix}}_{\boldsymbol{A}_d} \underbrace{\begin{bmatrix} \boldsymbol{\theta}(t_k^-) \\ \dot{\boldsymbol{\theta}}(t_k^-) \end{bmatrix}}_{\boldsymbol{x}(t_k^-)} + \underbrace{\begin{bmatrix} \boldsymbol{0}_{3\times3} \\ \boldsymbol{I}^{-1} \end{bmatrix}}_{\boldsymbol{B}_d} \underbrace{[\boldsymbol{n}_k]}_{\boldsymbol{v}_k}, \quad t = t_k
$$

(6b)

where Eq. (6a) is for the continuous portion, whereas Eq. (6b) describes the jump dynamics at the impulse instances. The vector quantity $\boldsymbol{x}(t)$ is the state, and $\boldsymbol{u}(t)$ and $\boldsymbol{v}_k$ are the continuous and impulsive control inputs, respectively. A total of N impulses are applied at time instances t_k, $k \in \{1, 2, \ldots, N\}$; and t_k^- and t_k^+ denote the instants right before and right after the impulse application, respectively. Assuming small angles and rates, $\boldsymbol{\theta} \approx \boldsymbol{\omega}$ and $\dot{\boldsymbol{\theta}} \approx 2\boldsymbol{\epsilon}$. It is also assumed that $\boldsymbol{m}$ will be small.

B. Selection of Impulse Application Times Based on Controllability

To find the best times t_k at which impulses should be applied, a comprehensive study is required on how the cost function defined in Sec. III.C (which depends on both the control efforts and the states) changes as a function of t_k. This study is beyond the scope of this Note, which focuses on optimal control given a set of prescribed impulse times, and it is part of the future work. Interested readers are referred to [13], which studied the necessary and sufficient optimality conditions for thruster firing times in formation flight applications and will be used as a basis for future work on this magnetic attitude control problem.

Within the scope of this Note, one reasonable approach to determine a prescribed set of times is to employ the thrusters only at the time instances at which the magnetic actuators are least capable of controlling the spacecraft. This approach may not be optimal in terms of fuel consumption and control effort (depending on the penalties specified by the designer), but it is expected to result in improvements in terms of attitude pointing performance by using thrusters to compensate for the lack of control authority of the magnetic controller.

The pointwise control authority of the system is assessed by computing the controllability Gramian over small time windows of width Δt spanning the total travel time. The impulse application times are then judiciously selected by determining when the smallest eigenvalue of this matrix reaches the local minima over each orbit (which indicates the times with the least control authority [7]):

$$
\boldsymbol{W}_j = \int_{\bar{t}_j}^{\bar{t}_j + \Delta t} e^{((\bar{t}_j + \Delta t) - \tau)\boldsymbol{A}_c} \boldsymbol{B}_c(\tau) \boldsymbol{B}_c^T(\tau) e^{((\bar{t}_j + \Delta t) - \tau)\boldsymbol{A}_c^T} \, d\tau \quad (7)
$$

where $\boldsymbol{W}_j$ is the controllability Gramian over the jth time window, starting from $\bar{t}_j$. Note that these $\bar{t}_j$ do not necessarily coincide with the impulse application times t_k. The matrices $\boldsymbol{A}_c$ and $\boldsymbol{B}_c(t)$ are the state-space matrices defined previously in Eq. (6a).

C. Design of the Hybrid Linear Quadratic Regulator

The hybrid performance index is defined as follows:

$$
J = \frac{1}{2}\boldsymbol{x}^T(t_f)\boldsymbol{S}\boldsymbol{x}(t_f) + \frac{1}{2}\int_0^{t_f} \boldsymbol{x}^T(t)\boldsymbol{Q}_c\boldsymbol{x}(t) + \boldsymbol{u}^T(t)\boldsymbol{R}_c\boldsymbol{u}(t)\, dt
$$
$$
+ \frac{1}{2}\sum_{k=1}^{N}[\boldsymbol{x}^T(t_k^-)\boldsymbol{Q}_d\boldsymbol{x}(t_k^-) + \boldsymbol{v}_k^T\boldsymbol{R}_d\boldsymbol{v}_k] \quad (8)
$$

where t_f refers to the end time, and $\boldsymbol{S} = \boldsymbol{S}^T \geq 0$ sets the terminal state penalty. The matrices $\boldsymbol{Q}_c = \boldsymbol{Q}_c^T \geq 0$ and $\boldsymbol{R}_c = \boldsymbol{R}_c^T > 0$ set the continuous state and control penalties, respectively; and $\boldsymbol{Q}_d = \boldsymbol{Q}_d^T \geq 0$ and $\boldsymbol{R}_d = \boldsymbol{R}_d^T > 0$ scale the discrete state and control penalties at the impulse instants, respectively. All penalty matrices were selected to be constant in this work.

As described in more detail in [7], using calculus of variations and setting the first variation of J to zero yields a set of conditions that, assuming a linear relationship between the states and the costates that are used to adjoin the continuous and impulsive dynamics, provides the following time-varying and discrete-time matrix Riccati equations:

$$
\dot{\boldsymbol{P}}(t) = -[\boldsymbol{P}(t)\boldsymbol{A}_c + \boldsymbol{A}_c^T\boldsymbol{P}(t) - \boldsymbol{P}(t)\boldsymbol{B}_c(t)\boldsymbol{R}_c^{-1}\boldsymbol{B}_c^T(t)\boldsymbol{P}(t) + \boldsymbol{Q}_c],
$$
$$
\boldsymbol{P}(t_f) = \boldsymbol{S} \quad (9a)
$$

$$
\boldsymbol{P}(t_k^-) = \boldsymbol{Q}_d + \boldsymbol{P}(t_k^+) - \boldsymbol{P}(t_k^+)\boldsymbol{B}_d(\boldsymbol{R}_d + \boldsymbol{B}_d^T\boldsymbol{P}(t_k^+)\boldsymbol{B}_d)^{-1}\boldsymbol{B}_d^T\boldsymbol{P}(t_k^+)
$$

(9b)

where $\boldsymbol{P}(t)$ describes the linear relationship between $\boldsymbol{x}(t)$ and the continuous costate, whereas $\boldsymbol{P}(t_k^+)$ describes that between $\boldsymbol{x}(t_k^+)$ and the discrete costate. Note that the discrete portion in Eq. (9b) has been simplified, with $\boldsymbol{A}_d$ being the identity in this case.

Lastly, after some further manipulation of the optimality conditions and using the aforementioned solution of the Riccati equations, the optimal continuous- and discrete-time feedback control inputs are given by

$$
\boldsymbol{u}^*(t) = -\boldsymbol{R}_c^{-1}\boldsymbol{B}_c^T(t)\boldsymbol{P}(t)\boldsymbol{x}(t) \quad (10a)
$$

$$
\boldsymbol{v}_k^* = -\boldsymbol{R}_d^{-1}\boldsymbol{B}_d^T\boldsymbol{A}_d^{-T}[\boldsymbol{P}(t_k^-) - \boldsymbol{Q}_d]\boldsymbol{x}(t_k^-) \quad (10b)
$$

The continuous Riccati equation in Eq. (9a) is integrated backward in time (as only the end condition is specified by the user). At each impulse, a jump is induced in the solution based on the discrete-time Riccati equation in Eq. (9b), and the computed $\boldsymbol{P}(t_k^-)$ value is used as a new terminal condition for Eq. (9a) to be integrated backward from t_k^- and t_{k-1}^+. This process is repeated until time zero, and since the time-varying system associated with the spacecraft considered in this Note is periodic over 15 orbits (and quasi periodic over one orbit), the resulting $\boldsymbol{P}(t)$ solution will lead to a periodic steady-state solution that can be approximated using Fourier series to reduce the storage memory requirements. It is important, however, to ensure that the number of terms in the series is sufficiently large to accurately capture the exact solution.

When simulating the nonlinear dynamics (together with the disturbance torques) in Eq. (1), starting with initial conditions at time zero, the Riccati solution $\boldsymbol{P}(t)$ and its value immediately before each impulse are used to compute, using Eqs. (10a) and (10b), the magnetic dipole moments and thruster gains that yield an optimal combination.

IV. Hybrid Linear Stability Analysis

The system in Eq. (6) in this attitude control problem is periodic, as long as the spacecraft is sufficiently close to Earth. Variations result over time from the time-varying nature of the magnetic field and Earth's tilt, but for a near-polar orbit, these variations are dominated by the spacecraft's orbital motion [14]. For the simulations presented in this Note, almost exact periodicity was observed with 15 orbits; but, in general, for low-Earth-orbit spacecraft that are close to being polar, the periodicity can be closely approximated to occur with one orbital period [3]. The stability analysis proposed in this section is independent of how many orbits are taken as the system's periodicity; but, for simplicity of exposition, periodicity with one orbit is assumed. The novel notion of hybrid Floquet analysis is then

proposed as an extension of the classical Floquet analysis used for linear time-periodic systems. This concept is then employed for assessing the linear stability of the system while integrating forward in the simulations.

Substituting the control inputs of Eq. (10) into Eq. (6) and rearranging yields

$$\dot{x}(t) = \tilde{A}_c(t)x(t) \triangleq [A_c - B_c(t)R_c^{-1}B_c^T(t)P(t)]x(t), \qquad t \neq t_k \tag{11a}$$

$$\begin{aligned}
x(t_k^+) &= \tilde{A}_{dk}x(t_k^-) \\
&\triangleq [A_d - B_d R_d^{-1}B_d^T A_d^{-T}(P(t_k^-) - Q_d)]x(t_k^-), \qquad t = t_k
\end{aligned} \tag{11b}$$

This suggests the use of the following continuous-time and discrete-time state transition matrices, which are then "patched" together to yield a hybrid matrix:

$$\begin{aligned}
\dot{\Phi}_k(t, t_{k-1}^+) &= [A_c - B_c R_c^{-1}B_c^T P]\Phi_k(t, t_{k-1}^+), \\
\Phi_k(t_{k-1}^+, t_{k-1}^+) &= 1, \qquad t \in (t_{k-1}, t_k)
\end{aligned} \tag{12a}$$

$$\Psi_k = [A_d - B_d R_d^{-1}B_d^T A_d^{-T}(P(t_k^-) - Q_d)], \qquad t = t_k \tag{12b}$$

Note that the time dependence of $B_c(t)$ and $P(t)$ has been omitted for clarity. To slightly simplify the notation, the second argument of the continuous state transition matrix will also be omitted, as the reference point is implied by the subscript k; that is, $\Phi_k(t) \triangleq \Phi_k(t, t_{k-1}^+)$. Starting from time $t_0^+ = 0$ with impulses at $t_k \in (0, T)$, $k \in \{1, 2, \cdots, \hat{N}\}$, until $t_{\hat{N}+1}^- = T$, one can relate the state within the κth interval (between $t_{\kappa-1}$ and t_κ) of the first orbit to the initial state as follows:

$$\begin{aligned}
x(t) &= \Phi_\kappa(t)x(t_{\kappa-1}^+) = \Phi_\kappa(t)\Psi_{\kappa-1}x(t_{\kappa-1}^-) \\
&= \Phi_\kappa(t)\Psi_{\kappa-1}\Phi_{\kappa-1}(t_{\kappa-1}^-)\ldots\Psi_2\Phi_2(t_2^-)\Psi_1\Phi_1(t_1^-)x_0
\end{aligned} \tag{13}$$

since $\Phi_1(t_1^-)x_0 = \Phi_1(t_1^-, 0^+)x_0 = x(t_1^-)$, based on Eqs. (11a) and (12a); then, $\Psi_1\Phi_1(t_1^-)x_0 = \Psi_1 x(t_1^-) = x(t_1^+)$ from Eqs. (11b) and (12b), and so on. The following theorem generalizes the Floquet theorem to hybrid systems, and it is proved in an analogous manner.

Theorem 1: Consider the following hybrid matrix constructed from those given by Eq. (12):

$$\begin{aligned}
\Xi(t) &\triangleq \Phi_\kappa(t)\Psi_{\kappa-1}\Phi_{\kappa-1}(t_{\kappa-1}^-) \cdots \Psi_2\Phi_2(t_2^-)\Psi_1\Phi_1(t_1^-), \\
\kappa &\in \{1, 2, \cdots, \hat{N}+1\}, \qquad t \in [t_{\kappa-1}, t_\kappa)
\end{aligned} \tag{14}$$

where $t_0^+ = 0$ and $t_{\hat{N}+1}^- = T$. If Ψ_κ is invertible for all $\kappa < \hat{N}+1$, then the following parts are true:

1) $\Xi(t)$ is a state transition matrix for the system in Eq. (11) such that $x(t) = \Xi(t)x_0$.

2) Assuming the system in Eq. (11) is periodic with period T and the impulse pattern is identical in all orbits, $\Xi(t+T) \triangleq \Xi(t)\Xi(T)$ is also a fundamental matrix solution of the system in Eq. (11). In addition, there exist a constant complex matrix Γ and an invertible T-periodic $\Delta(t)$, such that $\Xi(t) = \Delta(t)e^{t\Gamma}$.

Proof of part 1: Between impulses where $t \neq t_k$, differentiating $\Xi(t)$ with respect to time and realizing that its only time-varying constituent is $\Phi_\kappa(t)$ (as all the other ones have been computed at impulse times $\{t_1, \cdots, t_{\kappa-1}\}$), we have

$$\begin{aligned}
\dot{\Xi}(t) &= \dot{\Phi}_\kappa(t)\Psi_{\kappa-1}\Phi_{\kappa-1}(t_{\kappa-1}^-) \cdots \Psi_1\Phi_1(t_1^-), \\
\kappa &\in \{1, 2, \ldots, \hat{N}+1\}, \qquad t \in (t_{\kappa-1}, t_\kappa)
\end{aligned} \tag{15}$$

where, from Eq. (12a) and using the definition of $\tilde{A}_c(t)$ in Eq. (11a), we have $\dot{\Phi}_\kappa(t) = \tilde{A}_c(t)\Phi_\kappa(t)$. Substituting this back into Eq. (15) yields

$$\begin{aligned}
\dot{\Xi}(t) &= \tilde{A}_c(t)\Phi_\kappa(t)\Psi_{\kappa-1}\Phi_{\kappa-1}(t_{\kappa-1}^-) \cdots \Psi_1\Phi_1(t_1^-) \\
&= \tilde{A}_c(t)\Xi(t), \qquad t \in (t_{\kappa-1}, t_\kappa)
\end{aligned} \tag{16}$$

At impulse times $t = t_k$ (or, equivalently, $t = t_{\kappa-1}$ where κ denotes the interval between two impulses), we have

$$\begin{aligned}
\Xi(t_{\kappa-1}^+) &= \Phi_\kappa(t_{\kappa-1}^+)\Psi_{\kappa-1}\Phi_{\kappa-1}(t_{\kappa-1}^-) \cdots \Psi_1\Phi_1(t_1^-), \\
\kappa &\in \{1, 2, \cdots, \hat{N}+1\}
\end{aligned} \tag{17}$$

where, from Eq. (12b) and using the definition of $\tilde{A}_{dk}$ in Eq. (11b), we have $\Psi_{\kappa-1} = \tilde{A}_{d(\kappa-1)}$. Furthermore, from the initial condition of Eq. (12a), $\Phi_\kappa(t_{\kappa-1}^+) \triangleq \Phi_\kappa(t_{\kappa-1}^+, t_{\kappa-1}^+) = 1$ by construction. Substituting these back into Eq. (17) yields

$$\begin{aligned}
\Xi(t_{\kappa-1}^+) &= \tilde{A}_{d(\kappa-1)}\Phi_{\kappa-1}(t_{\kappa-1}^-)\Psi_{\kappa-2}\Phi_{\kappa-2}(t_{\kappa-2}^-) \cdots \Psi_1\Phi_1(t_1^-) \\
&= \tilde{A}_{d(\kappa-1)}\Xi(t_{\kappa-1}^-), \qquad t = t_{\kappa-1}
\end{aligned} \tag{18}$$

Comparing the results in Eqs. (16) and (18) with Eqs. (11a) and (11b), respectively, one concludes that $\Xi(t)$ as defined in Eq. (14) is a matrix solution of the system in Eq. (11). We now study the invertibility of this hybrid matrix by taking its determinant:

$$\begin{aligned}
\det\{\Xi(t)\} &= \det\{\Phi_\kappa(t)\} \times \det\{\Psi_{\kappa-1}\} \times \det\{\Phi_{\kappa-1}(t_{\kappa-1}^-)\} \\
&\times \cdots \times \det\{\Psi_1\} \times \det\{\Phi_1(t_1^-)\}
\end{aligned} \tag{19}$$

Since $\Phi_\kappa(t_\kappa^-)$ is a classical continuous state transition matrix satisfying Eq. (11a), from appendix A of [12], we can write

$$\det\{\Phi_\kappa(t)\} = \det\{\Phi_\kappa(t_{\kappa-1}^+)\}^{\nearrow 1} \times \exp\left\{\int_{t_{\kappa-1}^+}^t \text{trace}\{\tilde{A}_c(\tau)\}\,d\tau\right\} \tag{20}$$

where the exponential term on the right-hand side will not be zero for finite time; as a result, $\det\{\Phi_\kappa(t)\} \neq 0$ for all $\kappa \in \{1, 2, \cdots, \hat{N}+1\}$. Returning to Eq. (19), and imposing this theorem's condition that all Ψ_k are also invertible, it follows that $\det\{\Xi(t)\} \neq 0$; so, its columns are linearly independent. Together with the previous result that $\Xi(t)$ is a matrix solution of the system in Eq. (11), this means it is indeed a fundamental matrix solution of this system. Furthermore, one can write $x(t) = \Xi(t)x_0$ as demonstrated in Eq. (13), so $\Xi(t)$ is a state transition matrix, as required.

Proof of part 2: Hitherto, only the first orbit has been considered and $\Xi(t)$ has been defined for $t \in [0, T]$ only. However, assuming an identical impulse pattern over all orbits, the exact same patching procedure as that in Eq. (13) can be used to transform the state from that at the beginning of an arbitrary orbit (treated as the initial state) to any other time within that orbit. With the impulse times represented more generally as $t_k + \beta T$, $\beta \in \{0, 1, 2, \cdots\}$, the definitions in Eqs. (12a) and (12b) will be equally applicable to $t \in (t_{k-1} + \beta T, t_k + \beta T)$ and $t = t_k + \beta T$, respectively, producing Φ_k and Ψ_k identical to those in the first orbit. Taking note of this fact and considering only the second orbit without loss of generality, for $\tau \in (T, 2T]$, we have $x(\tau) = x(t + T) = \Xi(t)x(T)$, $t \in [0, T]$; but, from part 1, $x(T) = \Xi(T)x_0$ which implies that $x(t+T) = \Xi(t)\Xi(T)x_0$. Thus, the definition of $\Xi(t)$ in Eq. (14) can be augmented to also cover the second orbit by letting $\Xi(t+T) \triangleq \Xi(t)\Xi(T)$.

Between impulses where $t \neq t_k + T$, differentiating $\Xi(t+T)$ with respect to time, realizing that $\Xi(T)$ is a constant matrix computed at time T, and making use of Eq. (16), we have

$$\dot{\Xi}(t+T) = \dot{\Xi}(t)\Xi(T) = \tilde{A}_c(t)\Xi(t)\Xi(T) = \tilde{A}_c(t)\Xi(t+T) \tag{21}$$

At impulse times $t = t_k + T$, by using Eq. (18), we can write
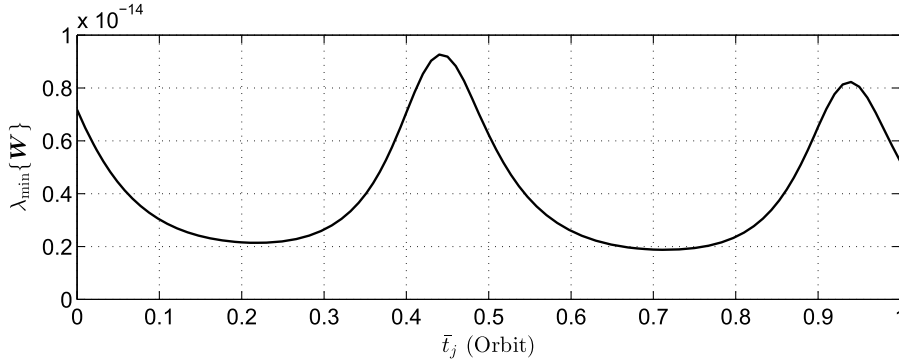
Fig. 1 Smallest eigenvalue of Gramian matrix (over $t \in [\bar{t}_j, \bar{t}_j + 0.05T]$).

$$\Xi((t_k + T)^+) = \Xi(t_k^+ + T) = \Xi(t_k^+)\Xi(T) = \tilde{A}_{dk}\Xi(t_k^-)\Xi(T)$$
$$= \tilde{A}_{dk}\Xi(t_k^- + T) = \tilde{A}_{dk}\Xi((t_k + T)^-) \qquad (22)$$

Since the system in Eq. (6) is assumed to be T periodic, $\tilde{A}_c(t) = \tilde{A}_c(t + T)$; and $\tilde{A}_{dk}$ is the same for both $t = t_k$ and $t = t_k + T$. Applying the change of variable $\tau \triangleq t + T$, Eqs. (21) and (22) can be rewritten as $\dot{\Xi}(\tau) = \tilde{A}_c(\tau)\Xi(\tau)$, when $\tau \neq t_k + T$, and $\Xi(\tau^+) = \tilde{A}_{dk}\Xi(\tau^-)$, when $\tau = t_k + T$. Thus, $\Xi(t + T)$ is a matrix solution of the system in Eq. (11), and since both $\Xi(t)$ and $\Xi(T)$ are invertible from part 1, $\Xi(t + T)$ is also a fundamental matrix solution of Eq. (11). The same applies for any $\Xi(t + \beta T)$.

Lastly, it is well known that any nonsingular $n \times n$ matrix can be written as e^{Γ}, where Γ is another $n \times n$ matrix that may be complex. In this case, let Γ be such that $e^{T\Gamma} = \Xi(T)$ and define $\Delta(t) \triangleq \Xi(t)e^{-t\Gamma}$. Then,

$$\Delta(t + T) = \Xi(t + T)e^{-(t+T)\Gamma} = \Xi(t)\Xi(T)e^{-T\Gamma}e^{-t\Gamma} = \Xi(t)e^{-t\Gamma} = \Delta(t) \qquad (23)$$

which means $\Delta(t)$ is also T periodic and, by its definition, $\Xi(t) = \Delta(t)e^{t\Gamma}$, as required. □

$\Xi(T)$ is henceforth termed the "hybrid state transition matrix." Assuming periodicity with T and the same impulse pattern in all orbits, the state at time $\tau = t + \beta T$, $\beta \in \{0, 1, 2, \cdots\}$ is given by $x(\tau) = \Xi(t)\Xi^{\beta}(T)x_0$. The eigenvalues of $\Xi(T) = \Delta(T)e^{T\Gamma}$ are the system's characteristic multipliers, whereas those of Γ are the system's characteristic (Floquet) exponents. Since $\Xi(t)$ has been shown to exhibit all properties of a classical state transition matrix, the following result applies analogously and can be used as a stability analysis tool:

Theorem 2: Let $x \equiv 0_{n \times 1}$ be the zero solution of the T-periodic system in Eq. (11). Consider $\Xi(t)$, a hybrid state transition matrix (defined by Eq. (14) for $t \in [0, T]$ and $\Xi(t + \beta T) = \Xi(t)\Xi^{\beta}(T)$, $\beta \in \{0, 1, 2, \cdots\}$), such that $x(\tau) = \Xi(\tau)x_0$ for all $\tau \in \mathbb{R}^+$. Let λ_i be the eigenvalues of $\Xi(t)$, and define $\lambda_{\max} = \max\{|\lambda_i|\}$, $i \in \{1, 2, \cdots, n\}$. Then, the following holds:

1) The solution $x \equiv 0$ is Lyapunov stable if $\lambda_{\max} \lesssim 1$.
2) The solution $x \equiv 0$ is asymptotically stable if $\lambda_{\max} < 1$.
3) The solution $x \equiv 0$ is unstable if $\lambda_{\max} > 1$.

Proof: Refer to section 2.4 of [15].

In the context of the attitude control problem of interest, since $b_G(t) = b_G(t + 15T) \approx b_G(t + T)$, we consequently have $B_c(t) = B_c(t + 15T) \approx B_c(t + T)$. In addition A_c, B_c, and B_d are constant, so the system in Eq. (6) is periodic. If the impulses are applied with the same period as that of the system, then Theorem 1 will hold, and the hybrid Floquet analysis can be applied. In the following section (Numerical Examples, Sec. V), the system's quasi periodicity over $1T$ is assumed, and the impulses are repeated with the same pattern at every orbit; therefore, the conditions required by Theorems 1 and 2 are satisfied.

V. Numerical Examples

The performance and stability of the proposed hybrid magnetic LQR controller were studied via simulations. The nonlinear attitude dynamics and kinematics given by Eqs. (1) and (5) were integrated numerically using the fourth-order Runge–Kutta algorithm and, at each time step, the total applied torque was computed via Eq. (3). The optimal control torques were based on Eq. (10), which were in turn computed using the steady-state $P(t)$ solution resulting from backward integration of the Riccati equations in Eq. (9). Residual magnetic dipole moments of $m_{\mathrm{dist}} = [0.1 \quad 0.1 \quad 0.1]^T \mathrm{A} \cdot \mathrm{m}^2$ were considered.

A circular near-polar Keplerian orbit with $e = 0$, $i = 87$ deg, $\Omega = 0$ rad, $\omega = 0$ rad, and $t_0 = 0$ s was considered with $a = 6.821 \times 10^6$ m, which corresponds to an altitude of 450 km. The spacecraft was assumed to have $I = \mathrm{diag}\{27, 17, 25\} \mathrm{kg} \cdot \mathrm{m}^2$, and the initial conditions were set to $\epsilon_0 = 0$, $\eta_0 = 1$, and $\omega_0 = [0.02\ 0.02\ 0.02]^T$ rad/s. For the purpose of quantifying some performance parameters (such as an estimation of the electrical energy consumption), the spacecraft was assumed to be equipped with three magnetic torquers with $R = 100\ \Omega$, $n = 400$ turns, $d = 10$ mm, and $A = (\pi d^2)/4$, based on some representative missions considered in [1].

The penalty matrices used for computing the hybrid performance index in Eq. (8) were tuned to produce satisfactory performance. The ratio between Q_c and R_c (as well as that between Q_d and R_d) determined the relative influence of the state and control penalties in the optimization process. For instance, in the limiting case of $Q_d = 0_{6 \times 6}$ and a very large R_d, the discrete states were not penalized, whereas any thruster control efforts were severely penalized, hence turning the hybrid controller into a purely magnetic one that did not use any thrusters. To somewhat reduce the design space and allow for tuning using scalar variables, the state penalty matrices were set to $Q_c = \mathrm{blockdiag}\{q_c \cdot 1_{3 \times 3}, q_c \cdot I\}$ and $Q_d = \mathrm{blockdiag}\{q_d \cdot 1_{3 \times 3}, q_d \cdot I\}$, and the control penalty matrices were set to $R_c = r_c \cdot 1_{3 \times 3}$ and $R_d = r_d \cdot 1_{3 \times 3}$. Note that, with the selected Q, the quadratic form $1/2(x^T Q x)$ included $1/2(q\dot{\theta}^T I\dot{\theta})$, which was a measure of the rotational kinetic energy. Lastly, the terminal penalty was set to $S = P(t_f) = 0_{6 \times 6}$.

Like any other LQR problem, the scalar values of the penalties had to be tuned manually. Some consideration of the physics of the problem, however, might provide some general insight for good starting points. For instance, keeping in mind that, with n turns, $m(t) = nAi(t)$; three coils' electrical energy consumption is given by

$$E = 3R/(n^2 A^2) \int_0^T m^T m \, dt$$

and since, in this problem, the continuous control input is $u(t) = m(t)$, setting $r_c = 3R/(n^2 A^2)$ seems reasonable, as it implies that $1/2(u^T R_c u)$ is a measure of the energy consumption. For the representative spacecraft with the aforementioned coil parameters,
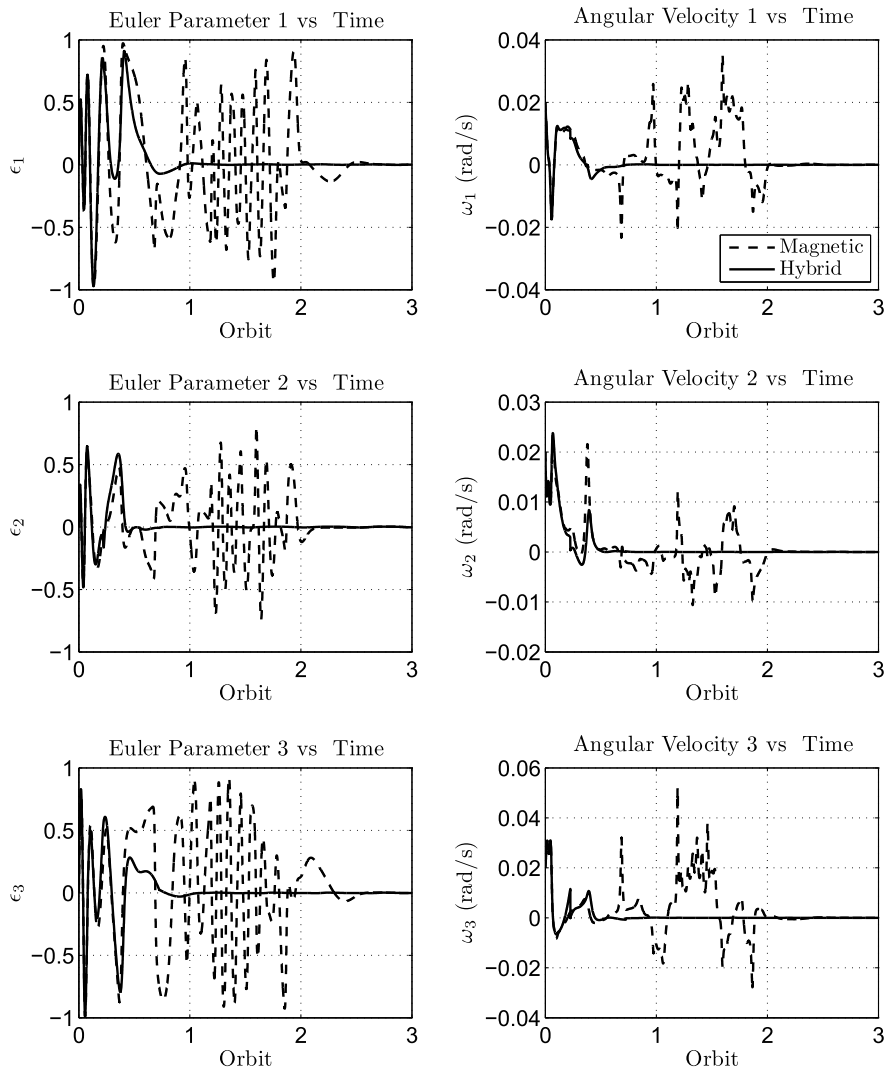
Fig. 2 Quaternions and angular velocity: solely magnetic (dashed) vs hybrid (solid) LQR ($r_c = 3 \times 10^5$ and $q_c = 10^8$; for hybrid, also $r_d = 10^{13}$ and $q_d = 10^{10}$).

$3R/(n^2 A^2) \approx 3.03 \times 10^5$. The penalty values for the hybrid LQR controller are set to $r_c = 3 \times 10^5$, $q_c = 10^8$, $r_d = 10^{13}$, and $q_d = 10^{10}$.

As a means of comparison, a solely magnetic LQR controller was also designed using a similar but continuous-only LQR approach (with no impulses applied). To this end, only Eqs. (9a) and (10a) were used, without a need for their discrete-time counterparts. To allow for a meaningful comparison between the two controllers' cost functions, the same continuous penalties as those of the hybrid controller (namely, $r_c = 3 \times 10^5$ and $q_c = 10^8$) were used for the solely magnetic LQR's design.

Shown in Fig. 1 is the evolution of the smallest eigenvalue of the controllability Gramian computed over small time windows (in this case, $\Delta t = 0.05T$) using Eq. (7). Lack of control authority is most evident over time windows starting with $\bar{t}_j = 0.21T$ and $\bar{t}_j = 0.71T$, with the same pattern repeating over the subsequent orbits. This suggests selecting the impulse application times such that they fall within these time windows. These are the times at which the spacecraft approaches Earth's poles. For this example, therefore, the impulses were applied at $t_k = 0.225T + (k-1) \times 0.5T$, $k \in \{1, 2, \cdots, N\}$.

Figure 2 shows the simulation results for the vector part of the quaternions and angular velocity of the spacecraft over three orbits, comparing the performance of the proposed hybrid LQR controller against that of a solely magnetic LQR controller (with no impulsive thrusting) as they attempt to drive the attitude from initial conditions to equilibrium ($\boldsymbol{\epsilon}_e = \mathbf{0}$, and $\boldsymbol{\omega}_e = [0 \ \ 0 \ \ 0]^T$ rad/s). It must be noted that, although the control laws were designed and implemented assuming $\dot{\boldsymbol{\theta}} \approx \boldsymbol{\omega}$ and $\boldsymbol{\theta} \approx 2\boldsymbol{\epsilon}$, the simulations used the full nonlinear

dynamics. The results suggested significant improvement achieved in terms of settling time and transient dynamics by augmenting the magnetic controller with impulsive thrusting for this particular choice of penalty matrices and impulse application times. The control torques applied by the magnetic torquers and thrusters are also shown in Fig. 3, from which considerable reduction in the magnetic control effort of the hybrid controller (albeit at the cost of additional thruster torques) is evident.

To provide a quantitative means of assessing the controller performance, the following norms were defined and computed over 10 orbits. These parameters provide rms-like measures of continuous torques, impulsive torques, angular velocities, and rotation angles, respectively. To compute the rotation angle, $\cos(\phi) = 1/2(\text{trace}\{C_{\text{BG}}\} - 1)$ was used after determination of the transformation matrix C_{BG}. The results, together with the total hybrid cost [given by Eq. (8)] and electrical energy consumption of the magnetic torquers assumed in this example, are listed in Table 1:

$$\|\boldsymbol{\tau}\|_{10T} = \sqrt{\frac{\int_0^{10T} \boldsymbol{\tau}_{\text{mag}}^T \boldsymbol{\tau}_{\text{mag}} \, dt}{10T}}, \qquad \|\boldsymbol{\omega}\|_{10T} = \sqrt{\frac{\int_0^{10T} \boldsymbol{\omega}^T \boldsymbol{\omega} \, dt}{10T}}$$

$$\|\boldsymbol{v}\|_{10T} = \sqrt{\frac{\int_0^{10T} \boldsymbol{\tau}_{\text{imp}}^T \boldsymbol{\tau}_{\text{imp}} \, dt}{10T}}, \qquad \|\boldsymbol{\phi}\|_{10T} = \sqrt{\frac{\int_0^{10T} \phi^2 \, dt}{10T}}$$

Although $\boldsymbol{\tau}_{\text{imp}}$ contains the Dirac delta function, the parameter $\|\boldsymbol{v}\|_{10T}$ is computed using a finite-width rectangular approximation of
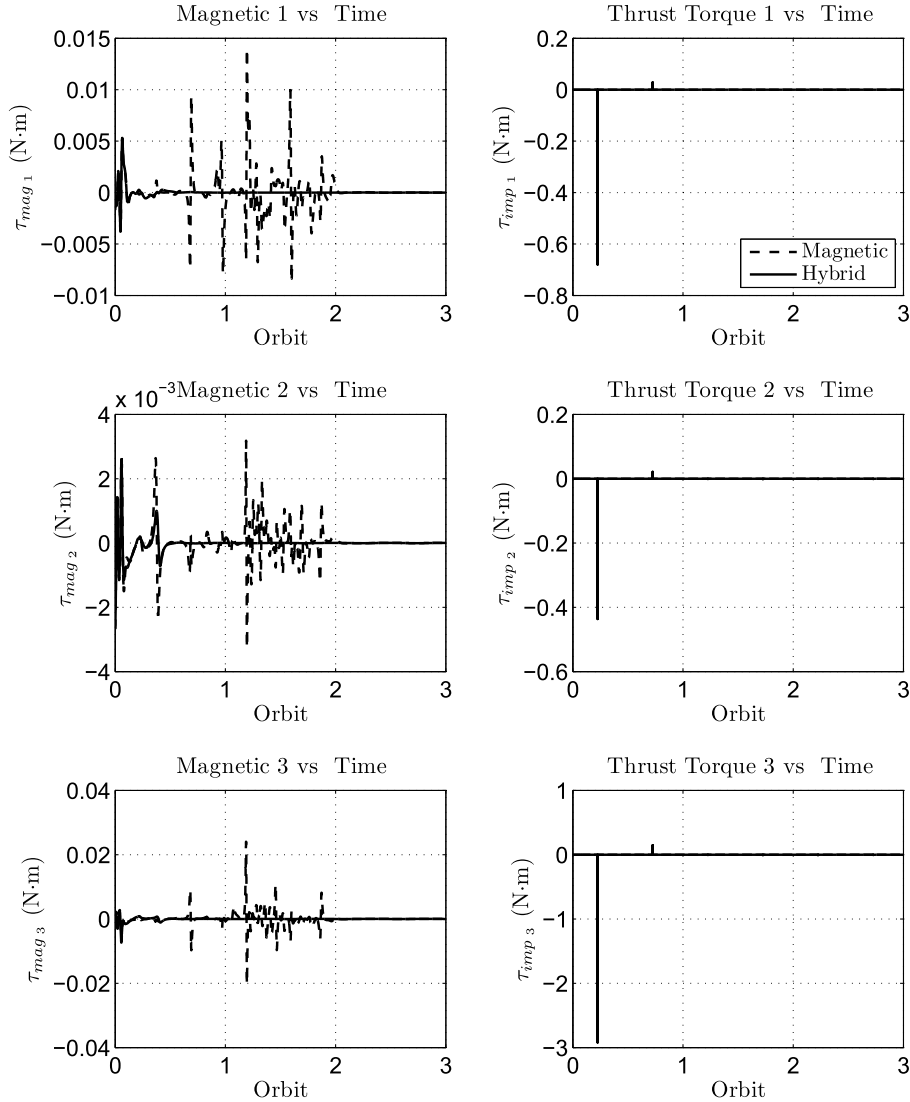
Fig. 3   Continuous and impulsive control torques: solely magnetic (dashed) vs hybrid (solid) LQR ($r_c = 3 \times 10^5$ and $q_c = 10^8$; for hybrid, also $r_d = 10^{13}$ and $q_d = 10^{10}$).

it, with height n_k/h and width h. Also included in Table 1 are the performance results using the proportional-derivative (PD) magnetic state-feedback controller proposed in [4], which is used as a benchmark for assessing the performance of the proposed hybrid LQR controller, as well as that of the solely magnetic controller using the same continuous-time penalty matrices as the hybrid one. To this end, the reference's control law $\boldsymbol{u} = \boldsymbol{m} = \boldsymbol{b}_B^{\times}\boldsymbol{\nu}/|\boldsymbol{b}_G|^2$ is used, where $\boldsymbol{\nu} = -(\gamma^2 k_p \boldsymbol{\epsilon} + \gamma k_v \boldsymbol{I} \boldsymbol{\omega})$. Since the same spacecraft moment of inertia matrix and orbital parameters as those in this Note were used in [4], the scaling parameter and gains are set to $\gamma = 0.001$ and

$k_p = k_v = 50$, which were the values reported in that paper. Both of the LQR controllers show significant attitude performance improvement compared to the reference PD controller, and the hybrid LQR exhibits improvements in terms of energy consumption and applied magnetic torques.

The proposed hybrid linear stability analysis approach described in Sec. IV was applied to the numerical example under study in this section. The periodicity of the system was assumed to be one orbit, and the continuous-time and discrete-time state transition matrices were computed based on Eq. (12). Lastly, the hybrid state transition matrix

Table 1   Comparison of performance of reference PD (based on [4]) vs solely magnetic and hybrid LQR controllers over $10T$[a]

Parameter	Description	Reference PD	Magnetic	Hybrid	Unit
J_{10T}	Total performance index	N/A[b]	2.77×10^{13}	2.99×10^{12}	— —
E_{10T}	Electrical energy consumption	7.66×10^6	5.35×10^7	4.40×10^6	MJ
$\|\boldsymbol{\tau}\|_{10T}$	Norm of magnetic torque	5.42×10^{-4}	1.54×10^{-3}	3.97×10^{-4}	N · m
$\|\boldsymbol{v}\|_{10T}$	Norm of impulsive torque	0	0	4.05×10^{-3}	N · m
$\|\boldsymbol{\omega}\|_{10T}$	Norm of angular velocity	4.54×10^{-3}	7.51×10^{-3}	3.51×10^{-3}	rad/s
$\|\boldsymbol{\phi}\|_{10T}$	Norm of rotation angle	1.84×10^0	8.83×10^{-1}	4.41×10^{-1}	rad

[a]PD: $\gamma = 0.001$ and $k_p = k_v = 50$; LQR: $r_c = 3 \times 10^5$ and $q_c = 10^8$; hybrid LQR: $r_c = 3 \times 10^5$, $q_c = 10^8$, $r_d = 10^{13}$, and $q_d = 10^{10}$.
[b]N/A denotes "not applicable."

Table 2   Eigenvalue magnitudes of hybrid state transition matrix $\Xi(T)$

Controller	$|\lambda_1|$	$|\lambda_2|$	$|\lambda_3|$	$|\lambda_4|$	$|\lambda_5|$	$|\lambda_6|$
Magnetic	4.33×10^{-3}	2.17×10^{-8}	2.17×10^{-8}	1.86×10^{-9}	1.80×10^{-11}	1.80×10^{-11}
Hybrid	1.86×10^{-3}	1.76×10^{-8}	1.76×10^{-8}	1.83×10^{-9}	1.98×10^{-11}	9.75×10^{-12}

was constructed using Eq. (14), and its eigenvalues were computed to draw conclusions regarding the linear stability of the system.

For the hybrid case with impulses applied at $t_1 = 0.225T$ and $t_2 = 0.725T$ in the first orbit, both of the discrete state transition matrices were computed to be of full rank, $\mathrm{rank}\{\Psi_2\} = \mathrm{rank}\{\Psi_1\} = 6$, and well conditioned, $\mathrm{cond}\{\Psi_1\} \approx 4.17$ and $\mathrm{cond}\{\Psi_2\} \approx 4.14$. Therefore, both matrices were determined to be invertible, hence satisfying the conditions of Theorem 1 and producing an invertible hybrid state transition matrix: $\Xi(T) = \Phi_3(T, t_2^+)\Psi_2\Phi_2(t_2^-, t_1^+)\Psi_1\Phi_1(t_1^-, 0)$.

The eigenvalues of $\Xi(T)$ are the characteristic multipliers of the hybrid system and, based on the extension of the Floquet stability theory given in Theorem 2, the periodic system is stable (in the linear region) if all of these eigenvalues are within the unit circle. Listed in Table 2 are the magnitudes of the eigenvalues of $\Xi(T)$ for both the solely magnetic [for which $\Xi(T) = \Phi(T, 0)$, as there are no impulses] and hybrid LQR controllers used in this numerical example. Both control schemes result in eigenvalues less than unity, which implies that both should be able to asymptotically stabilize the system as long as the initial conditions are within a sufficiently small neighborhood of the equilibrium state.

VI.   Conclusions

A novel attitude control strategy using magnetic torquers and impulsive thrusters in tandem has been presented, in which a hybrid (continuous/impulsive) linear quadratic regulator (developed in [7]) has been used to determine the optimal control signals that minimized a hybrid cost function. The use of an auxiliary impulsive thrust mechanism was primarily intended to overcome the limited gain margin of a solely magnetic scheme. A controllability-based study has been suggested for judicious selection of the impulse application times, but further analytical and numerical studies on optimizing the impulse application times and number of impulses would be worthwhile. Moreover, a treatment of the novel concept of hybrid Floquet analysis has been presented and used for studying the stability of the proposed hybrid controller. Numerical simulation results showed improved control performance and significant reduction of magnetic control effort, at least for a specific choice of penalties and impulse times, which would be particularly advantageous for missions that had relatively strict pointing accuracy requirements.

References

[1] Wertz, J. R., *Spacecraft Attitude Determination and Control*, D. Reidel Publishing Co, Dordrecht, The Netherlands, 1978, Chap. 19.

[2] Silani, E., and Lovera, M., "Magnetic Spacecraft Attitude Control: A Survey and Some New Results," *Control Engineering Practice*, Vol. 13, No. 3, March 2005, pp. 357–371.
doi:10.1016/j.conengprac.2003.12.017

[3] Wiśniewski, R., "Linear Time-Varying Approach to Satellite Attitude Control Using Only Electromagnetic Actuation," *Journal of Guidance, Control, and Dynamics*, Vol. 23, No. 4, July–Aug. 2000, pp. 640–647.
doi:10.2514/2.4609

[4] Lovera, M., and Astolfi, A., "Spacecraft Attitude Control using Magnetic Actuators," *Automatica*, Vol. 40, No. 8, Aug. 2004, pp. 1405–1414.
doi:10.1016/j.automatica.2004.02.022

[5] Psiaki, M. L., "Magnetic Torquer Attitude Control via Asymptotic Periodic Linear Quadratic Regulation," *Journal of Guidance, Control, and Dynamics*, Vol. 24, No. 2, March–April 2001, pp. 386–394.
doi:10.2514/2.4723

[6] Lovera, M., and Astolfi, A., "Global Magnetic Attitude Control of Inertially Pointing Spacecraft," *Journal of Guidance, Control, and Dynamics*, Vol. 28, No. 5, Sept.–Oct. 2005, pp. 1065–1072.
doi:10.2514/1.11844

[7] Sobiesiak, L. A., and Damaren, C. J., "Optimal Continuous/Impulsive Control for Lorentz-Augmented Spacecraft Formations," *Journal of Guidance, Control, and Dynamics*, Vol. 38, No. 1, Jan. 2015, pp. 151–157.
doi:10.2514/1.G000334

[8] Damaren, C. J., "Hybrid Magnetic Attitude Control Gain Selection," *Journal of Aerospace Engineering*, Vol. 223, No. 8, Aug. 2009, pp. 1041–1047.
doi:10.1243/09544100JAERO641

[9] Forbes, J. R., and Damaren, C. J., "Linear Time-Varying Passivity-Based Attitude Control Employing Magnetic and Mechanical Actuation," *Journal of Guidance, Control, and Dynamics*, Vol. 34, No. 5, Sept.–Oct. 2011, pp. 1363–1372.
doi:10.2514/1.51899

[10] Pulecchi, T., and Lovera, M., "Attitude Control of Spacecraft with Partially Magnetic Actuation," *IFAC Proceedings Volumes, 17th IFAC Symposium on Automatic Control in Aerospace*, Vol. 17, No. 1, 2007, pp. 609–614.
doi:10.3182/20070625-5-FR-2916.00104

[11] Pulecchi, T., Lovera, M., and Varga, A., "Optimal Discrete-Time Design of Three-Axis Magnetic Attitude Control Laws," *IEEE Transactions on Control Systems Technology*, Vol. 18, No. 3, May 2010, pp. 714–722.
doi:10.1109/TCST.2009.2024757

[12] Hughes, P. C., *Spacecraft Attitude Dynamics*, Wiley, New York, 1986, Chap. 4.

[13] Sobiesiak, L. A., and Damaren, C. J., "Lorentz-Augmented Spacecraft Formation Reconfiguration," *IEEE Transactions on Control Systems Technology*, Vol. 24, No. 2, Aug. 2016, pp. 514–524.

[14] Wiśniewski, R., and Blanke, M., "Fully Magnetic Attitude Control for Spacecraft Subject to Gravity Gradient," *Automatica*, Vol. 35, No. 7, July 1999, pp. 1201–1214.
doi:10.1016/S0005-1098(99)00021-7

[15] Chicone, C., *Ordinary Differential Equations with Applications*, 2nd ed., Springer–Verlag, New York, 2006, Sec. 2.4.
doi:10.1007/0-387-35794-7